The aged rhesus macaque manifests Braak stage III/IV Alzheimer's-like pathology

Constantinos D. Paspalas[a,*], **Becky C. Carlyle**[b], **Shannon Leslie**[b], **Todd M. Preuss**[c], **Johanna L. Crimins**[a], **Anita J. Huttner**[d], **Christopher H. van Dyck**[a,b,e], **Douglas L. Rosene**[f], **Angus C. Nairn**[b], and **Amy F. T. Arnsten**[a,b,**]

[a]Department of Neuroscience, Yale School of Medicine, New Haven, CT, USA

[b]Department of Psychiatry, Yale School of Medicine, New Haven, CT, USA

[c]Division of Neuropharmacology and Neurologic Diseases, Yerkes National Primate Center, Emory University, Atlanta, GA, USA

[d]Department of Pathology, Yale School of Medicine, New Haven, CT, USA

[e]Department of Neurology, Yale School of Medicine, New Haven, CT, USA

[f]Department of Anatomy and Neurobiology, Boston University School of Medicine, Boston, MA, USA

Abstract

Introduction: An animal model of late-onset Alzheimer's disease is needed to research what causes degeneration in the absence of dominant genetic insults and why the association cortex is particularly vulnerable to degeneration.

Methods: We studied the progression of tau and amyloid cortical pathology in the aging rhesus macaque using immunoelectron microscopy and biochemical assays.

Results: Aging macaques exhibited the same qualitative pattern and sequence of tau and amyloid cortical pathology as humans, reaching Braak stage III/IV. Pathology began in the young-adult entorhinal cortex with protein kinase A-phosphorylation of tau, progressing to fibrillation with paired helical filaments and mature tangles in oldest animals. Tau pathology in the dorsolateral prefrontal cortex paralleled but lagged behind the entorhinal cortex, not afflicting the primary visual cortex.

Discussion: The aging rhesus macaque provides the long-sought animal model for exploring the etiology of late-onset Alzheimer's disease and for testing preventive strategies.

*Corresponding author. Tel.: +1-203-785-5230; Fax: + 1-203-785-5263. **Corresponding author. Tel.: +1-203-785-4431; Fax: +1-203-785-5263.

1. Introduction

Tauopathy is the hallmark of Alzheimer's disease (AD), caused by abnormal phosphorylation/aggregation of the microtubule-associated tau protein; hyperphosphorylated tau fibrillates as paired helical filaments (PHFs) in neurofibrillary tangles (NFTs) [1–3]. NFTs accumulate within degenerating neurons and correlate with cognitive deficits [4,5]. In late-onset AD, fibrillated tau immunoreactivity first arises in the "cell islands" of the layer II entorhinal cortex (ERC; Braak stage I/II), with the earliest signs of labeled neurites evident in young-middle age (Braak stage Ia/b). Pathology continues to worsen in the ERC and begins in the pyramidal neurons of the association cortex, for example, the dorsolateral prefrontal cortex (dlPFC; Braak stage III/IV), progressing to involve the primary visual cortex (V1) at end-stage disease (Braak stage V/VI) [1,5,6]. Braak stage III/IV associates primarily with memory impairments, befitting the extensive degeneration in the ERC, whereas explicit dementia is associated with Braak stage V/VI, when there is extensive degeneration in the association cortices [5]. Amyloidosis, the other hallmark pathology in AD, is caused by amyloid β (Aβ) peptides deposited extracellularly in senile plaques. Aβ is generated after the sequential cleavage of amyloid precursor protein (APP) by β- and γ-secretase in the endocytotic amyloidogenic pathway [7,8]. Unlike NFTs, the amyloid load correlates weakly with cognitive deficits [4,5], but refer to the study by Murphy and Levine [9].

In vitro and transgenic mouse models have transformed AD research, revealing how genetic insults lead to tau and amyloid pathology in familial early-onset AD [10]. However, genetic models do not address questions pertaining to the native course of the most common, late-onset AD. Why does advancing age lead to the same phenotype as dominantly heritable early-onset disease, and why does AD present a specific pattern and sequence of degeneration that progresses along interconnected glutamatergic neurons in the association cortex [11]? These questions require a model species with extensive association cortex, where both tau and amyloid pathologies arise naturally with advancing age.

While nonhuman primates have extensive association cortex and manifest amyloid pathology similar to humans, early research failed to detect AD-like tau pathology with neuronal degeneration (reviewed in [12]), supporting the hypothesis that AD is a phylogenetic, human-specific disease [13]. There is since a single report of true tau pathology with PHFs in the prefrontal cortex of a chimpanzee [14], but hominids are not available for invasive research. We studied rhesus macaques from young to extreme old age (up to 38 years of age) using immunoelectron microscopy to capture early stages of tau phosphorylation and its progression to fibrillation in the ERC and dlPFC. We report that aging macaques exhibit the same qualitative pattern and sequence of tau pathology as humans, reaching Braak stage III/IV in the oldest animals. Perfusion-fixation of the brain

allowed the visualization of early tau pathology as well as tracing of the amyloidogenic pathway *in situ*, which is unprecedented and not possible in humans after death. We propose that the aging rhesus macaque can model the development of AD pathology, recapitulating those early, preclinical events that initiate age-related degeneration.

2. Methods

All procedures were approved by the Boston, Emory, and Yale Universities and National Institute on Aging Institutional Animal Care and Use Committees and conformed to the Guide for the Care and Use of Laboratory Animals of the Office of Laboratory Animal Welfare, National Institutes of Health.

2.1. Biochemical assays

Brain samples from 11 rhesus macaques (aged 4.5–31 years) of the Yale and Emory Universities' brain collections were used for the biochemical assays. Animals and tissue sampling procedures are described in Supplementary Methods.

2.1.1. Tau fractionation—Flash-frozen tissue was homogenized in Tris-buffered saline (TBS; 50 mM Tris pH 7.4, 274 mM NaCl, 5 mM KCl, plus cOmplete EDTA-free protease inhibitor and PhosSTOP [Roche, Indianapolis, IN] phosphatase inhibitor). The homogenate was centrifuged at $150,000 \times g$ for 20 minutes at 4°C, and the supernatant was removed and frozen as the S1 TBS-soluble tau fraction. The pellet was resuspended in P1 buffer (0.8 M NaCl, 10% sucrose, 10 mM Tris pH 7.4, 1 mM EGTA, and cOmplete protease inhibitor) and respun under the same conditions. The S2 supernatant was removed, and sarkosyl added to a final concentration of 1%. The supernatant was heated for 1 hour at 37°C and centrifuged for 1 hour at $150,000 \times g$ at 4°C, yielding a supernatant containing salt-extractable tau and S3, and a pellet containing P3 sarkosyl-insoluble tau. P3 sarkosyl-insoluble tau was not detected in either the ERC or dlPFC.

2.1.2. Immunoblotting—A rabbit polyclonal antibody against human tau (Dako A0024; Agilent, Santa Clara, CA) was used for all immunoblots. The primary antibody was visualized with the IRDye 680 anti-rabbit secondary antibody in the Odyssey infrared scanner (LI-COR Biosciences, Lincoln, NE). Bands were quantified using ImageJ (National Institutes of Health), and correlation analysis was performed using Prism 7 (GraphPad, La Jolla, CA). Band proportion analysis was normalized within lane, representing the proportion of total tau in each band. Total tau measurements were normalized using Amido Black total protein stain (Sigma-Aldrich, St. Louis, MO). The membranes were visualized using the ChemiDoc instrument (Bio-Rad, Hercules, CA). After tau labeling, further analysis of the ERC blots was attempted that required stripping, and the Amido Black signal was poor thereafter. Therefore, a parallel check was performed to normalize the ERC data by running an input tau check (noncentrifuged homogenate). The same proportional patterns of total tau distribution were observed between fractions using this check.

2.2.   Light and electron immunomicroscopy

The brains of 10 rhesus macaques (aged 7–38 years) from four brain collections (Yale, Boston, and Emory Universities and the National Institute on Aging) were used for the anatomy studies. Animals including cognitive characterization (if applicable), anesthesia, and histological processing are described in Supplementary Methods.

2.2.1.   Antibodies—Primary antibodies were raised in rabbits or mice and complexed with species-specific goat secondary or tertiary antibodies. Primaries raised in different species were selected for dual immunocytochemistry.

The following primary antibodies against human proteins were used: (1) mouse anti-phosphoSer214-tau IgM (clone CP3) [15] at 1:200 (generously provided by Dr. Peter Davies, Litwin-Zucker Research Center); (2) mouse antiphosphoSer202 + Thr205-tau IgG_{1k} (clone AT8) at 1:300 (MN1020; Thermo Fisher Scientific, Waltham, MA); (3) mouse anti-phosphoThr181-tau IgG_{1k} (clone AT270) at 1:200 (MN1050; Thermo Fisher Scientific); (4) mouse anti-phosphoThr231-tau IgG_{1k} (clone AT180) at 1:200 (MN1040; Thermo Fisher Scientific); (5) rabbit anti-phosphoSer2808-RyR_2 IgG at 1:250 (ab59225; Abcam, Cambridge, MA); (6) rabbit anti-$A\beta_{1-42}$ IgG at 1:100 (AB5078P; EMD Millipore, Billerica, MA); (7) mouse anti-$A\beta_{1-42}$ IgG_{2b} (clone MOAB-2) at 1:300 (NBP2-13075; Novus, Littleton, CO); and (8) rabbit anti-APP (C-terminus) IgG at 1:600 (A8717; Sigma-Aldrich).

The following secondary and tertiary antibodies were used: goat anti-rabbit F(ab′)$_2$, biotin-conjugated, at 1:500 (Jackson ImmunoResearch Labs, West Grove, PA); (2) goat anti-mouse F(ab′)$_2$, biotin-conjugated, at 1:500 (Jackson ImmunoResearch Labs); (3) goat anti-rabbit Fab′, 1.4-nm gold cluster-conjugated, at 1:200 (Nanoprobes, Yaphank, NY); (4) goat anti-mouse Fab′, 1.4-nm gold cluster-conjugated, at 1:200 (Nanoprobes); and (5) goat anti-biotin IgG, 1.4-nm gold cluster-conjugated, at 1:300 (Nanoprobes).

2.2.2.   Single and dual immunocytochemistry—Sections underwent three freeze-thaw cycles in liquid nitrogen to permeabilize cell membranes and were subsequently processed free-floating for immunocytochemistry. Nonspecific reactivity was suppressed with 10% non-immune goat serum and 2% IgG-free bovine serum albumin (BSA) in 50 mM TBS. The sections were additionally treated with 0.5% sodium borohydride in TBS to quench nonreactive aldehydes before protein blocking. Normal sera and BSA were purchased from Jackson ImmunoResearch Labs. Acetylated BSA was from Aurion (Wageningen, The Netherlands). All chemicals and supplies for electron microscopy were purchased from Sigma-Aldrich and Electron Microscopy Sciences (Hatfield, PA), respectively.

For peroxidase single immunolabeling, sections were incubated for 36 hours at 4°C in primary antibodies in TBS plus 2% non-immune goat serum (NTBS) and transferred for 2 hours at room temperature (RT) to species-specific biotinylated F(ab′)$_2$ fragments in NTBS and finally to avidin-biotinylated peroxidase (1:200 in TBS; Vector, Burlingame, CA) for 2 hours at RT. Peroxidase activity was visualized in 0.05% diaminobenzidine (DAB) in TBS with the addition of 0.01% hydrogen peroxide for 8–12 minutes.

For gold single immunolabeling, antibodies were diluted in NTBS and applied for 36 hours at 4°C. The sections were washed in NTBS supplemented with 0.07% Tween 20 and 0.1% acetylated BSA (gold buffer) and incubated for 2 hours at RT with species-specific Fab′ conjugated to 1.4-nm gold cluster. After fixation in 1% buffered glutaraldehyde, gold was enhanced under a mercury-vapor safelight for 8–10 minutes on ice with a silver autometallographic developer (HQ Silver; Nanoprobes). Alternatively, after the biotinylated secondary antibody, the sections were incubated in 1.4-nm gold-conjugated anti-biotin IgG for 2 hours at RT and silver-enhanced as described previously.

For peroxidase-gold dual immunolabeling, sections were incubated for 48 hours at 4° C in a mixture of two primary antibodies. Secondary antibodies were used for 3 hours at RT as a mixture of species-specific 1.4-nm gold and biotin conjugates. Gold was silver-enhanced as in a single immunocytochemistry. The biotinylated antibodies were complexed with peroxidase and developed with the DAB chromogenic reaction as described previously. Alternatively, the labeling sequence was reversed, so that previously gold-labeled antigens were visualized with DAB, and vice versa.

For each immunocytochemical series, a parallel set of experiments controlled for cross-reactivities and methodological artifacts (Supplementary Methods). Labeled sections were processed for light and electron microscopy imaging as described in Supplementary Methods.

3. Results

3.1. Early development of tau pathology in the ERC

The rhesus macaque allows high-resolution, timely detection of phosphorylated yet not fibrilled tau species that degrade in humans after death. Tau normally functions to stabilize microtubules but detaches and aggregates when phosphorylated by cyclic adenosine monophosphate (cAMP)-protein kinase A (PKA) [15]. PKA-phosphorylated tau (pSer214-tau) was seen in layer II ERC cell islands in young-adult macaques (7–9 years; Fig. 1A), consistent with early tau pathology in the ERC of young-adult humans (Braak stage Ia/b). PKA-phosphorylated tau aggregated along microtubules in dendrites (Fig. 1B–D), "entrapping" transporting endosomes as captured in Fig. 1D. PKA-phosphorylated tau was also found in transporting endosomes and trafficked between neurons at plasma membrane endo/exocytotic profiles (Fig. 1E).

3.1.1. Tau pathology and Ca^{2+} dysregulation in the synapse—In the young-adult ERC, pSer214-tau aggregated within glutamatergic-like synapses onto dendrites and on smooth endoplasmic reticulum (SER) cisterns underneath the synapses. These Ca^{2+} storing SER elements were unique in that they were enlarged and extensively elaborated and often bridged the synapse to a mitochondrion (Fig. 1F and 1G). We have termed this SER specialization, by analogy with the spine apparatus, "dendritic subsynaptic reticulum" (DSR). The pairing of the DSR with the pSer214-tau-afflicted synapses suggests a possible involvement of internal Ca^{2+} in tau pathology. Supporting this hypothesis, PKA-phosphorylation of RyR$_2$ (pSer2808-RyR$_2$), which causes Ca^{2+} leak from the SER in

cardiac and brain cells [16,17], was found on the DSR cisterns (Fig. 1H and 1I), suggesting that dysregulated PKA-Ca^{2+} signaling may have an early role in instigating tau pathology.

3.2. Fibrillated tau in the ERC

The pattern and sequence of tau fibrillation in the aging macaques' cortex, revealed with the AT8 antibody against PHF-tau, corresponded to Braak staging of AD using the same antibody [6]. In "younger" aged macaques (24–26 years), there was mild AT8 reactivity in the outer tier of layer II stellate cell islands in the ERC, including in a 26-year-old macaque with confirmed cognitive deficits (Fig. 2A and Supplementary Table), consistent with Braak stage I/II. With still older age (33–34 years), AT8 labeling became intense and widespread throughout the cell islands of the layer II (Fig. 2B), with sporadic labeling of pyramidal cells in the deeper ERC (and dlPFC; see below), consistent with Braak stage III. In the oldest macaque examined, a 38-year-old macaque with pronounced cognitive deficits (Supplementary Table), mature NFTs were observed in both layer II (Fig. 2C) and layer V (Fig. 2D) ERCs, consistent with Braak stage III/IV.

To directly demonstrate fibrillated tau in aged macaques (33–34 years), we used high-power immunoelectron microscopy. Layer II ERC neurons contained loose fibrillar clusters that reacted with AT8 and other antibodies against human PHF-tau (Fig. 2E and 2F, and Supplementary Fig. 1), consistent with NFTs and neuropil threads. Fibrils were distinct from intermediate filaments in glia (Supplementary Fig. 2) and composed of straight and paired 10-nm filaments with abrupt endings and the typical 80-nm helical periodicity of PHFs in AD (Fig. 2G–I) [18]. Layer II ERC neurons also showed typical signs of AD-like degeneration, including large autophagic vacuoles in the soma and proximal dendrites (Fig. 2J and 2K), microglial engulfment, argyrophilia, massive accumulation of late-phase lysosomes, and dystrophic neurites (Fig. 3A–D). "Ghost dendrites" (Fig. 2K) were seen in AT8-reactive pretangle neurons, indicating severe cellular disruption before full NFT formation. Notably, pyramidal neurons in the layer V ERC of the same macaques displayed a "healthy" ultrastructure with no signs of vacuolar degeneration or autophagy (Supplementary Fig. 3).

Because the macaque data were obtained after transcardial fixation and zero postmortem interval (PMI), we tested how these conditions compare with conditions used in neuropathology. The brain of a 28-year-old macaque was removed after death (1 hour PMI) and immersion-fixed in buffered formalin, which is the routine processing of human brains. Even with this short PMI, the new protocol resulted in the dissolution of most of AT8-immunoreactivity in the ERC, likely due to loss of partially fibrillated tau from pretangle neurons (Supplementary Fig. 4).

3.3. Tau pathology in the dlPFC

In humans, tau pathology extends from the ERC to the association cortex with advancing age. The pattern is similar in aging macaques, with tau phosphorylation appearing in the association cortex at a later age than in the ERC. Thus, pSer214-tau is detected in pyramidal neurons of the aged dlPFC (31–34 years; Fig. 4A), but not in the young-adult dlPFC [19] or in resilient primary cortices (Supplementary Fig. 5). Labeling was found in spines at

glutamatergic-like synapses and over the spine apparatus, similar to pSer214-tau aggregating over synapses and the DSR in ERC dendrites (compare Fig. 4B to Fig. 1F).

Consistent with a later appearance of tau phosphorylation in the association cortex, tau fibrillation was only sporadic in the aged dlPFC (Fig. 4C). AT8 labeled PHFs (Fig. 4D and 4E), consistent with Braak stage III/IV. Biochemical assays confirmed that tau phosphorylation is less advanced in the dlPFC than in the ERC (Fig. 4F and 4G, Supplementary Figs. 6 and 7), similar to the progression of tau pathology in aging humans.

3.4. Amyloid pathology and endosomal trafficking

Amyloid pathology was also observed in aged macaques. However, despite peak fibrillary pathology and neuronal degeneration, the layer II ERC showed minimal amyloidosis, with most of the extracellular amyloid deposits found in the layer V, similar to the pattern in the human ERC. Labeling against $A\beta_{1-42}$ revealed parenchymal amyloid plaques with a fibrous core composed of straight, unbranching 10-nm fibrils corresponding to fibrous amyloid (Fig. 5A–C) as well as extensive vascular amyloid deposition (not shown). Intracellular $A\beta$ was found in endosomes localized next to mitochondria (Fig. 5D), a likely site of γ-secretase activity [20], and on the plasma membrane in dendrites and axons (Fig. 5E and 5F). Such membrane appositions of $A\beta$ endosomes may be capturing release into the intercellular space, for example, from an axon in Fig. 5F.

In vitro studies have shown that "entrapping" APP in endosomes drives cleavage to $A\beta$ [21]. In the macaque, phosphorylated tau surrounds endosomes and potentially hinders transport along the microtubules, both in early stages of phosphorylation (Fig. 1D) and in later fibrillated states (Fig. 5G). To determine whether these endosomes may contain APP, we double labeled for APP and AT8. In the aged ERC, APP-transporting endosomes (please note the tagged C-terminus is on the cytoplasmic aspect of the endosomal membrane) were surrounded by fibrillated tau aggregates (Fig. 5H). Similarly in the dlPFC, APP was trafficked in endosomes (Fig. 6A–D) and internalized via clathrin-mediated endocytosis (Fig. 6B), as it is known from research *in vitro* [8]. As in the ERC, fibrillated tau aggregated on APP-transporting endosomes (Fig. 6E).

4. Discussion

This study reports that the aging rhesus macaque exhibits the qualitative pattern and sequence of tau and amyloid pathology observed in humans. Tau phosphorylation and fibrillation arise in the same cell types, layers and cortical regions, and in the same progressive sequence as in AD, reaching Braak stage III/IV in the oldest animals. Aged macaques manifested true AD-like tau pathology with mature NFTs and PHFs of the typical ultrastructure. Moreover, there are $A\beta$-reactive senile plaques and neurons undergoing vacuolar degeneration and autophagy. Taken together, the data establish the rhesus macaque as a valid animal model for late-onset AD. Pathology in humans is more extensive, as to be expected given the great expansion of association cortical connections and the longer lifespan.

In neuropathology, human AD brains are collected after death and immersion-fixed in formalin. Long PMI and formalin denature proteins and dramatically degrade the fine structure. Our own controls demonstrate that early species of phosphorylated tau are detected in the perfused macaque brain but lost after death. Thus, it is the nearly indestructible highly fibrillated tau that mostly survives in brain autopsies. Likewise, Aβ and APP along the endocytotic pathway cannot be visualized in humans because of the loss of antigenicity and the extensive damage of endomembranes (e.g., Golgi and SER cisterns and the endosomal compartment) that occur after death. In other words, early pathology, which is lost in routine neuropathological examination, may be the key to illuminating the etiology of the disease.

In contrast, the macaque brain is transcardially perfused with very potent fixatives to preserve both the fine structure and antigenicity. Using this model, we traced the trafficking of APP from the trans-Golgi to clathrin-coated membrane pits and into endosomes in neurites, which is known to be exacerbated by the apolipoprotein E4 (*APOE* ε4) genotype to increase Aβ production and risk of AD [22]. We have also captured Aβ in transporting endosomes in association with the plasma membrane, where Aβ soluble oligomers could be secreted into the intercellular space to have toxic effects on synapses [23]. Moreover, we documented dissemination of tau pathology, for example, pSer214-tau trafficking between neurons at endo/exocytotic appositions in the ERC (Fig. 1E) and dlPFC [19], consistent with tau "seeding" known from mouse AD models [24,25]. These observations *in situ* would support the diagnostic use of blood exosomes as early indicators of the intracellular milieu of afflicted neurons [26].

It is already known that Aβ can drive tau phosphorylation *in vivo* [27]. Our data in the ERC and dlPFC suggest that aggregated phosphorylated tau may "entrap" APP-transporting endosomes, thus retaining APP and intensifying its cleavage to Aβ similar to retromer insults [21], hence fueling a vicious cycle of degeneration; see [28] for a tau-amyloid unifying hypothesis. This may be key for late-onset AD, where tau pathology appears before amyloid pathology [1]. The early degeneration of the layer II ERC may destroy the "engine" for Aβ production, and so limited amyloidosis was found there, while the gradual tau pathology in the dlPFC may generate extensive amyloid load, for example, as seen with amyloid-binding positron emission tomography [29]. Varied preventive/therapeutic strategies may interrupt this vicious cycle, and the aging macaque would be a unique opportunity to rigorously test such strategies at prodromal stages of degeneration.

The aging macaque brain may be used to observe *in situ* molecular changes that initiate AD pathology in the absence of genetic insults. Researchers have long hypothesized that the degenerative process may be fueled by Ca^{2+} dysregulation [30–32]. A role for internal Ca^{2+} was encouraged by the discovery that presenilins, the catalytic core in the γ-secretase complex, facilitate Ca^{2+} efflux from SER stores [33]. Our discovery that pSer214-tau aggregates over the DSR and the spine apparatus, both Ca^{2+}-storing SER specializations in ERC dendrites and dlPFC spines, respectively, supports Ca^{2+} involvement. Further support is added by our finding that DSR cisterns display PKA-phosphorylated RyR_2, known to cause Ca^{2+} leak [16,17]. In cardiac muscle, RyR_2 phosphorylation leads to Ca^{2+} overload of mitochondria, inflammation, and heart failure [34]. Similar actions in higher cortical circuits

with advancing age may also lead to mitochondrial dysfunction and inflammation, both associated with AD [35,36], as well as drive Aβ cleavage and tau phosphorylation [37–39]. Thus, the early appearance of pSer2808-RyR$_2$ in the macaque's ERC may model the increased RyR Ca^{2+} signaling in the human cortex during early phases of tau phosphorylation (Braak stage I/II) [40] and the increased Ca^{2+} flux through RyR$_2$ in young 3xTg mice before fibrillary pathology [41].

Studies of the aging macaque may finally help explain why the association cortex is particularly vulnerable to degeneration. Pyramidal cells in the newly evolved dlPFC communicate via immense numbers of corticocortical glutamatergic synapses on their spines [42] and develop excessive cAMP-PKA signaling with advanced age, related at least in part to the loss of the phosphodiesterase PDE4A [19]. PDE4D is also reduced with advancing age in the human dlPFC [43], suggesting that weaker regulation of cAMP in the aging dlPFC translates across primate species. Dorsolateral PFC glutamatergic synapses are regulated in a remarkable manner, whereby feedforward cAMP-Ca^{2+} signaling controls the open-state of hyperpolarization-activated cyclic nucleotide-gated and K$^+$ channels to dynamically gate network strength [44]. Layer II "grid cells" in the ERC also serve as a hub for association cortical connections [45], and, like dlPFC neurons, are dynamically modulated by cAMP-hyperpolarization-activated cyclic nucleotidegated channel signaling [46,47]. These glutamatergic synapses in the dlPFC and ERC are the foundation of flexible, higher cognition but may also serve as an engine of pathology when cAMP-Ca^{2+} signaling is not held in check. Importantly, the number of corticocortical synapses in dlPFC and ERC increases greatly over evolution—rodents << monkeys < apes < humans—corresponding to the degree of AD-like pathology in these species [42,48,49].

Supplementary Material

Refer to Web version on PubMed Central for supplementary material.

Acknowledgments

References

[1]. Braak H, Thal DR, Ghebremedhin E, Del Tredici K. Stages of the pathologic process in Alzheimer disease: age categories from 1 to 100 years. J Neuropathol Exp Neurol 2011;70:960–9. [PubMed: 22002422]

[2]. Iqbal K, Liu F, Gong CX. Tau and neurodegenerative disease: the story so far. Nat Rev Neurol 2016;12:15–27. [PubMed: 26635213]

[3]. Wang Y, Mandelkow E. Tau in physiology and pathology. Nat Rev Neurosci 2016;17:5–21. [PubMed: 26631930]

[4]. Giannakopoulos P, Herrmann FR, Bussieère T, Bouras C, Kövari E, Perl DP, et al. Tangle and neuron numbers, but not amyloid load, predict cognitive status in Alzheimer's disease. Neurology 2003; 60:1495–500. [PubMed: 12743238]

[5]. Nelson PT, Alafuzoff I, Bigio EH, Bouras C, Braak H, Cairns NJ, et al. Correlation of Alzheimer disease neuropathologic changes with cognitive status: a review of the literature. J Neuropathol Exp Neurol 2012; 71:362–81. [PubMed: 22487856]

[6]. Braak H, Alafuzoff I, Arzberger T, Kretzschmar H, Del Tredici K. Staging of Alzheimer disease-associated neurofibrillary pathology using paraffin sections and immunocytochemistry. Acta Neuropathol 2016;112:389–404.

[7]. LaFerla FK, Green KN, Oddo S. Intracellular amyloid-β in Alzheimer's disease. Nat Rev Neurosci 2007;8:499–509. [PubMed: 17551515]

[8]. O'Brien RJ, Wong PC. Amyloid precursorprotein processing and Alzheimer's disease. Annu Rev Neurosci 2011;34:185–204. [PubMed: 21456963]

[9]. Murphy MP, Levine H, 3rd. Alzheimer's disease and the β-amyloid peptide. J Alzheimers Dis 2010;19:311–23. [PubMed: 20061647]

[10]. Morrissette DA, Parachikova A, Green KN, LaFerla FM. Relevance of transgenic mouse models to human Alzheimer disease. J Biol Chem 2009;284:6033–7. [PubMed: 18948253]

[11]. Bussière T, Giannakopoulos P, Bouras C, Perl DP, Morrison JH, Hof PR. Progressive degeneration of nonphosphorylated neurofilament protein-enriched pyramidal neurons predicts cognitive impairment in Alzheimer's disease: stereologic analysis of prefrontal cortex area 9. J Comp Neurol 2003;463:281–302. [PubMed: 12820162]

[12]. Finch CE, Austad SN. Commentary: is Alzheimer's disease uniquely human? Neurobiol Aging 2015;36:553–5. [PubMed: 25533426]

[13]. Rapoport SI. Hypothesis: Alzheimer's disease is a phylogenetic disease. Med Hypotheses 1989;29:147–50. [PubMed: 2528670]

[14]. Rosen RF, Farberg AS, Gearing M, Dooyema J, Long PM, Anderson DC, et al. Tauopathy with paired helical filaments in an aged chimpanzee. J Comp Neurol 2008;509:259–70. [PubMed: 18481275]

[15]. Jicha GA, Weaver C, Lane E, Vianna C, Kress Y, Rockwood J, et al. cAMP-dependent protein kinase phosphorylations on tau in Alzheimer's disease. J Neurosci 1999;19:7486–94. [PubMed: 10460255]

[16]. Wehrens XH, Lehnart SE, Reiken S, Vest JA, Wronska A, Marks AR. Ryanodine receptor/ calcium release channel PKA phosphorylation: a critical mediator ofheart failure progression. Proc Natl Acad Sci USA 2006;103:511–8. [PubMed: 16407108]

[17]. Liu X, Betzenhauser MJ, Reiken S, Meli AC, Xie W, Chen BX, et al. Role of leaky neuronal ryanodine receptors in stress-induced cognitive dysfunction. Cell 2012;150:1055–67. [PubMed: 22939628]

[18]. Crowther RA. Straight and paired helical filaments in Alzheimer disease have a common structural unit. Proc Natl Acad Sci U S A 1991; 88:2288–92. [PubMed: 1706519]

[19]. Carlyle BC, Nairn AC, Wang M, Yang Y, Jin LE, Simen AA, et al. cAMP-PKA phosphorylation of tau confers risk for degeneration in aging association cortex. Proc Natl Acad Sci U S A 2014; 111:5036–41. [PubMed: 24707050]

[20]. Pavlov PF, Wiehager B, Sakai J, Frykman S, Behbahani H, Winblad B, et al. Mitochondrial γ-secretase participates in the metabolism of mitochondria-associated amyloid precursor protein. FASEB J 2011; 25:78–88. [PubMed: 20833873]

[21]. BhallaA VetanovetzCP, MorelE ChamounZ, Di PaoloG SmallSA. The location and trafficking routes of the neuronal retromer and its role in amyloid precursor protein transport. Neurobiol Dis 2012; 47:126–34. [PubMed: 22516235]

[22]. He X, Cooley K, Chung CH, Dashti N, Tang J. Apolipoprotein receptor 2 and X11 alpha/beta mediate apolipoprotein E-induced endocytosis of amyloid-beta precursor protein and beta-secretase, leading to amyloid-beta production. J Neurosci 2007;27:4052–60. [PubMed: 17428983]

[23]. Um JW, Kaufman AC, Kostylev M, Heiss JK, Stagi M, Takahashi H, et al. Metabotropic glutamate receptor 5 is a coreceptor for Alzheimer Aβ oligomer bound to cellular prion protein. Neuron 2013; 79:887–902. [PubMed: 24012003]

[24]. Liu L, Drouet V, Wu JW, Witter MP, Small SA, Clelland C, et al. Transsynaptic spread of tau pathology in vivo. PLoS One 2012;7:e31302. [PubMed: 22312444]

[25]. de Calignon A, Polydoro M, Suárez-Calvet M, William C, Adamowicz DH, Kopeikina KJ, et al. Propagation of tau pathology in a model of early Alzheimer's disease. Neuron 2012;73:685–97. [PubMed: 22365544]

[26]. Fiandaca MS, Kapogiannis D, Mapstone M, Boxer A, Eitan E, Schwartz JB, et al. Identification of preclinical Alzheimer's disease by a profile of pathogenic proteins in neurally derived blood exosomes: a case-control study. Alzheimers Dement 2015;11:600–7. [PubMed: 25130657]

[27]. Götz J, Chen F, van Dorpe J, Nitsch RM. Formation of neurofibrillary tangles in P301l tau transgenic mice induced by Aβ fibrils. Science 2001;293:1491–5. [PubMed: 11520988]

[28]. Small SA, Duff K. Linking Aβ and tau in late-onset Alzheimer's disease: a dual pathway hypothesis. Neuron 2008;60:534–42. [PubMed: 19038212]

[29]. Devanand DP, Mikhno A, Pelton GH, Cuasay K, Pradhaban G, Dileep Kumar JS, et al. Pittsburgh compound B (11C-PIB) and fluorodeoxyglucose (18 F-FDG) PET in patients with Alzheimer disease, mild cognitive impairment, and healthy controls. J Geriatr Psychiatry Neurol 2010;23:185–98. [PubMed: 20430977]

[30]. Camandola S, Mattson MP. Aberrant subcellular neuronal calcium regulation in aging and Alzheimer's disease. Biochim Biophys Acta 2011;1813:965–73. [PubMed: 20950656]

[31]. Woods NK, Padmanabhan J. Neuronal calcium signaling and Alzheimer's disease. Adv Exp Med Biol 2012;740:1193–217. [PubMed: 22453989]

[32]. Alzheimer's Association Calcium Hypothesis Workgroup. Calcium hypothesis of Alzheimer's disease and brain aging: a framework for integrating new evidence into a comprehensive theory of pathogenesis. Alzheimers Dement 2017;13:178–82. [PubMed: 28061328]

[33]. Zhang H, Sun S, Herreman A, De Strooper B, Bezprozvanny I. Role of presenilins in neuronal calcium homeostasis. J Neurosci 2010; 30:8566–80. [PubMed: 20573903]

[34]. Santulli G, Xie W, Reiken SR, Marks AR. Mitochondrial calcium overload is a key determinant in heart failure. Proc Natl Acad Sci U S A 2015;112:11389–94. [PubMed: 26217001]

[35]. Young-Collier KJ, McArdle M, Bennett JP. The dying of the light: mitochondrial failure in Alzheimer's disease. J Alzheimers Dis 2012;28:771–81. [PubMed: 22057028]

[36]. Li Y, Tan MS, Jiang T, Tan L. Microglia in Alzheimer's disease. Biomed Res Int 2014;2014:437483. [PubMed: 25197646]

[37]. Mattson MP, Engle MG, Rychlik B. Effects of elevated intracellular calcium levels on the cytoskeleton and tau in cultured human cortical neurons. Mol Chem Neuropathol 1991;15:117–42. [PubMed: 1663746]

[38]. Hayley M, Perspicace S, Schulthess T, Seelig J. Calcium enhances the proteolytic activity of BACE1:an in vitro biophysical and biochemical characterization of the BACE1-calcium interaction. Biochim Biophys Acta 2009;1788:1933–8. [PubMed: 19486882]

[39]. Hartigan JA, Johnson GV. Transient increases in intracellular calcium result in prolonged site-selective increases in Tau phosphorylation through a glycogen synthase kinase 3beta-dependent pathway. J Biol Chem 1999;274:21395–401. [PubMed: 10409701]

[40]. Kelliher M, Fastbom J, Cowburn RF, Bonkale W, Ohm TG, Ravid R, et al. Alterations in the ryanodine receptor calcium release channel correlate with Alzheimer's disease neurofibrillary and beta-amyloid pathologies. Neuroscience 1999;92:499–513. [PubMed: 10408600]

[41]. Chakroborty S, Goussakov I, Miller MB, Stutzmann GE. Deviant ryanodine receptor-mediated calcium release resets synaptic homeostasis in presymptomatic 3xTg-AD mice. J Neurosci 2009;29:9458–70. [PubMed: 19641109]

[42]. Elston GN, Benavides-Piccione R, Elston A, Zietsch B, Defelipe J, Manger P, et al. Specializations of the granular prefrontal cortex of primates: implications for cognitive processing. Anat Rec A Discov Mol Cell Evol Biol 2006;288:26–35. [PubMed: 16342214]

[43]. Lu T, Pan Y, Kao SY, Li C, Kohane I, Chan J, et al. Gene regulation and DNA damage in the ageing human brain. Nature 2004;429:883–91. [PubMed: 15190254]

[44]. Arnsten AF, Wang M, Paspalas CD. Neuromodulation of thought: flexibilities and vulnerabilities in prefrontal cortical network synapses. Neuron 2012;76:223–39. [PubMed: 23040817]

[45]. Insausti R, Amaral DG, Cowan WM. The entorhinal cortex of the monkey: II. Cortical afferents. J Comp Neurol 1987;264:356–95. [PubMed: 2445796]

[46]. Giocomo LM, Hussaini SA, Zheng F, Kandel ER, Moser MB, Moser EI. Grid cells use HCN1 channels for spatial scaling. Cell 2011;147:1159–70. [PubMed: 22100643]

[47]. Heys JG, Hasselmo ME. Neuromodulation of I(h) in layer II medial entorhinal cortex stellate cells: a voltage-clamp study. J Neurosci 2012;32:9066–72. [PubMed: 22745506]

[48]. Krimer LS, Hyde TM, Herman MM, Saunders RC. The entorhinal cortex: an examination of cyto- and myeloarchitectonic organization in humans. Cereb Cortex 1997;7:722–31. [PubMed: 9408036]

[49]. DeFelipe J The evolution of the brain, the human nature of cortical circuits, and intellectual creativity. Front Neuroanat 2011;5:29. [PubMed: 21647212]

RESEARCH IN CONTEXT

1. **Systemic review:** There is great need for an animal model of late-onset Alzheimer's disease with naturally developing pathology, to learn why advancing age increases risk of degeneration in highly interconnected neurons in the association cortex. Rhesus macaques have extensive association cortex; however, previous studies found amyloid plaques but not neurofibrillary tangles in the aged cerebral cortex.

2. **Interpretation:** We examined the association cortices of aging rhesus macaques, including macaques of extreme old age, and found evidence of paired helical filaments in mature neurofibrillary tangles in the oldest animals. The pattern and sequence of tau pathology was qualitatively similar to that in humans. Immunoelectron microscopy revealed early stages of tau and amyloid pathology, including evidence of dysregulated calcium signaling in the neural circuits subserving memory.

3. **Future directions:** Future research can use rhesus macaques to help reveal the etiology of Alzheimer's disease–like degeneration in the aging cortex and to test strategies for prevention.
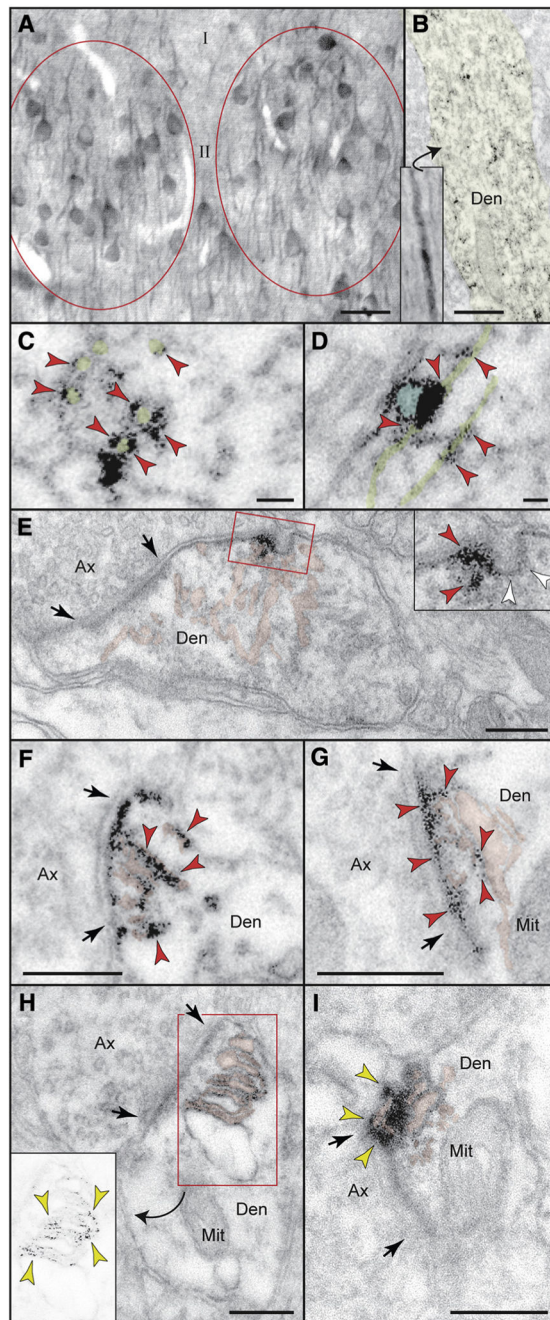
Fig. 1.
Tau phosphorylation in the layer II ERC of young-adult macaque (7–9 years). (A) Stellate cell islands (red ovals) react against pSer214-tau. (B) Correlated light/electron microscopy shows labeling in a principal dendrite (pseudocolored). (C and D) pSer214-tau-reactive microtubules (green-pseudocolored) in cross-sectioned (C) and longitudinally sectioned (D) dendrites; an endosome [cyan-pseudocolored in (D)] is "entrapped" along the microtubules by heavy aggregation of pSer214-tau. (E) Endo/exocytosis (frame and inset) of pSer214-tau; white arrowheads point to an omegashaped profile on the plasma membrane. The elaborate SER (see below) is pink-pseudocolored. (F and G) In ERC dendrites, both the synapse and

DSR (i.e., Ca^{2+}-storing SER expansion subjacent to glutamatergic-like synapses) accumulate pSer214-tau. (H and I) DSR cisterns but not the synapses react against pSer2808-RyR_2 (yellow arrowheads). Red arrowheads point to pSer214-tau; synapses are between arrows. Scale bars, 30 μm (A), 500 nm (B), 50 nm (C,D), 200 nm (E–I). Abbreviations: Ax, axon; Den, dendrite; DSR, dendritic subsynaptic reticulum; ERC, entorhinal cortex; Mit, mitochondrion; pSer214-tau, protein kinase A-phosphorylated tau; SER, smooth endoplasmic reticulum.
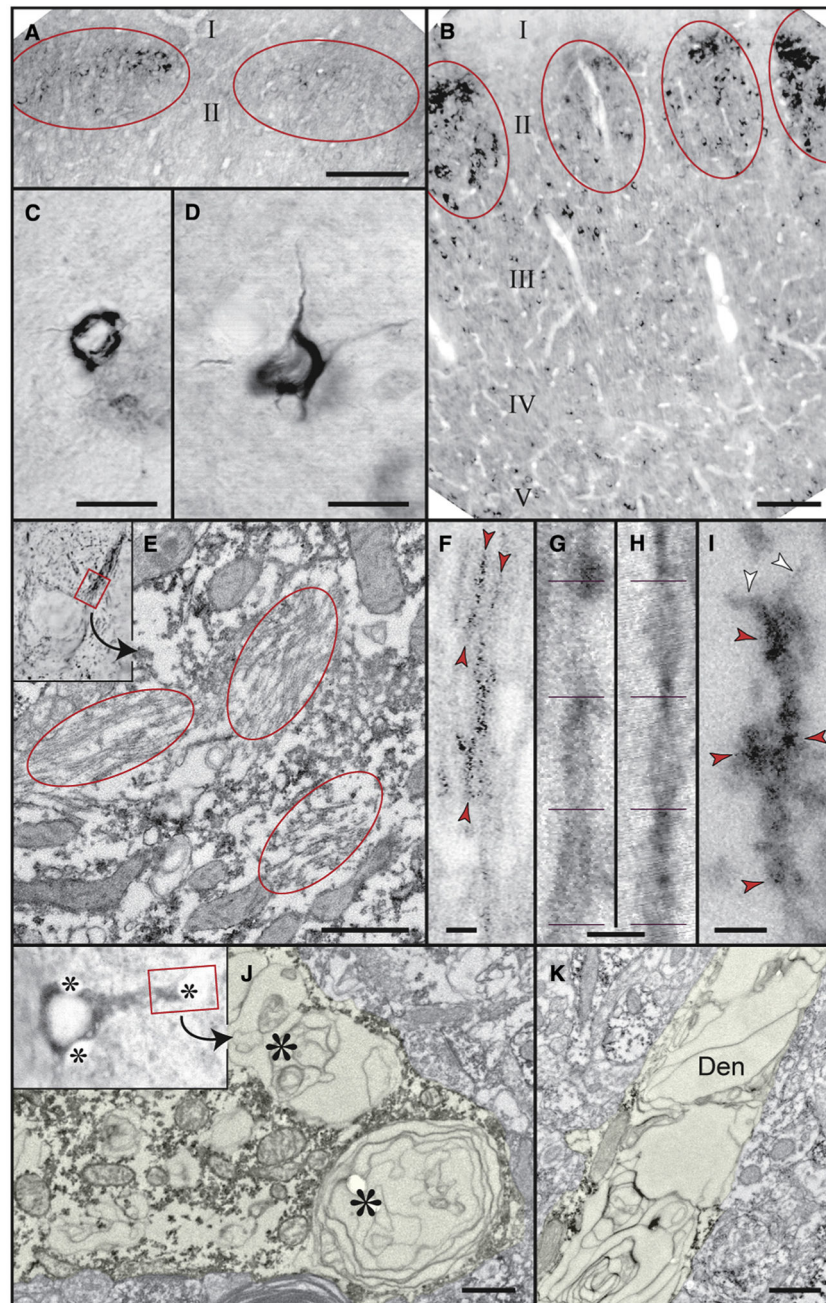
Fig. 2
. Tau fibrillation (AT8 labeling) in the aging macaque ERC. (A) Mild tau fibrillation is restricted in layer II cell islands (red ovals; 26 years). (B) Advanced fibrillation in layer II islands extends into the deeper ERC (33 years). (C and D) Mature NFTs in layer II (C) and layer V (D) ERCs (38 years). (E) Correlated light/electron microscopy reveals loose fibril bundles (red ovals) in the tapering proximal dendrite, consistent with NFTs (33 years). (F) Individual fibrils react against PHF-tau (red arrowheads). (G and H) High-power microscopy demonstrates 10-nm filament strands in a double-helix twist with a cross-over repeat of 80 nm (parallel bars), and with varying width of 10–22 nm (G), identical to PHFs in AD (H). (I)

AT8-reactive PHFs (red arrowheads) end abruptly, exposing paired 10-nm filament strands (white arrowheads; 34 years). (J) Correlated light/electron microscopy of a pretangle layer II stellate neuron (34 years). Asterisks mark autophagic vacuoles with multilamellar bodies in the soma and principal dendrite (pseudocolored). (K) "Ghost" dendrite (Den) of the degenerating neuron shown in (J); the entire cytoplasm is lysed. Scale bars, 100 μm (A and B), 10 μm (C and D), 500 nm (E, J, and K), 100 nm (F), 40 nm (G–I). Abbreviations: AD, Alzheimer's disease; ERC, entorhinal cortex; NFTs, neurofibrillary tangles; PHF, paired helical filament; pSer214-tau, protein kinase A-phosphorylated tau.
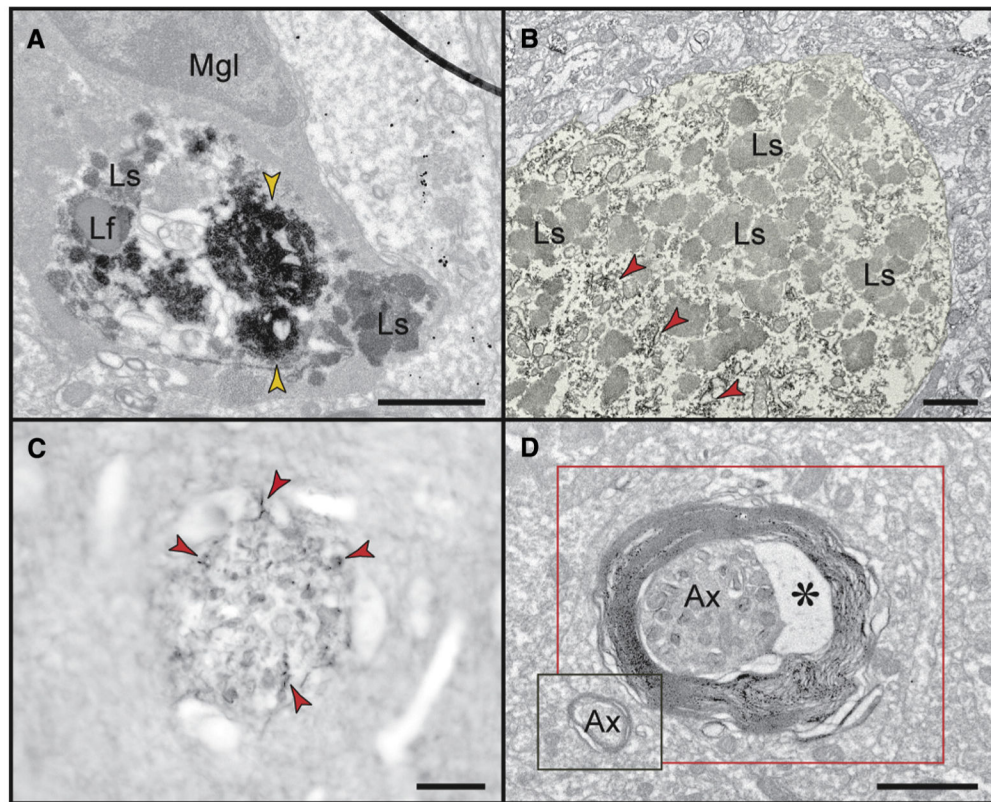
Fig. 3.
Neuronal degeneration in the layer II of the aged macaque ERC (33–34 years). (A)
Microglia (Mgl) engulfs a degenerating cellular profile containing large argyrophilic masses
(yellow arrowheads), numerous late-phase lysosomes (Ls), and lipofuscin inclusions (Lf).
(B) Detail of an AT8-labeled (red arrowheads) pretangle neuron (pseudocolored) with an
abnormal accumulation of late-phase lysosomes (Ls). (C) A senile plaque composed of AT8-
reactive dystrophic neurites (red arrowheads); compare with the senile plaque labeled
against Aβ in Fig. 5A. (D) A dystrophic myelinated axon (red frame) contains numerous
autophagosomes and a large vacuole in place of the inner mesaxon (asterisk). A second
myelinated axon of typical appearance (black frame) is shown for size comparison. Scale
bars, 1 μm (A, B, and D) and 30 μm (C). Abbreviations: Aβ, amyloid β; Ax, axon; ERC,
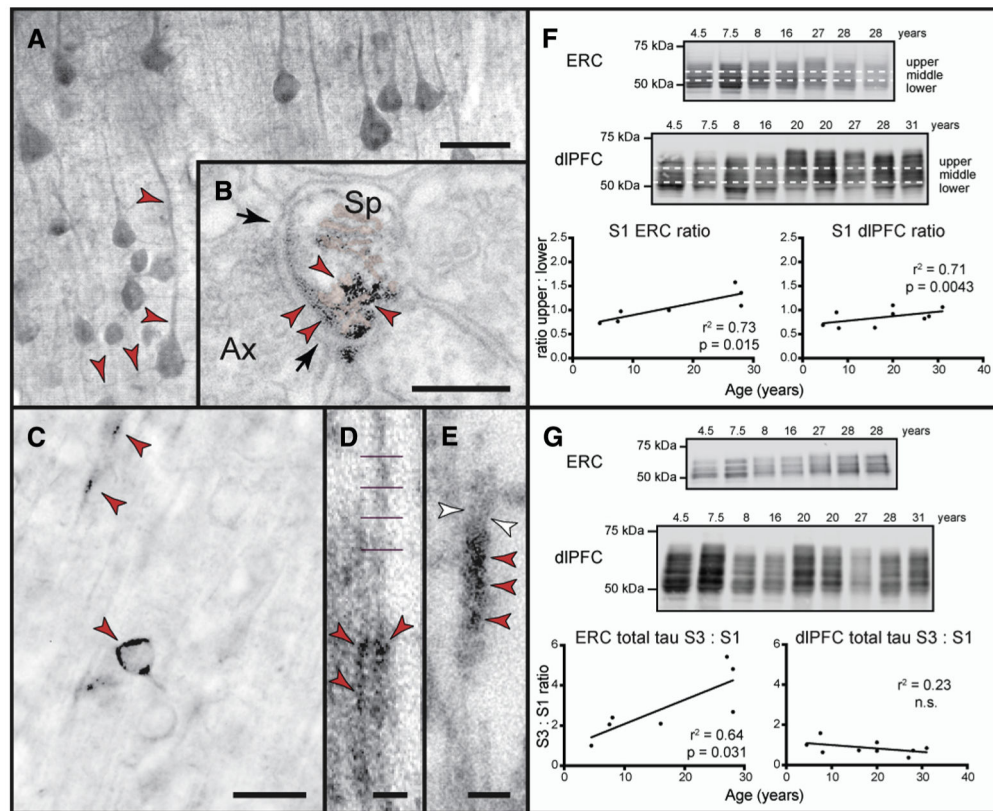entorhinal cortex.

Fig. 4.

The pattern and sequence of tau phosphorylation in the macaque dlPFC parallels but lags behind the ERC. (A) Layer III pyramidal neurons in the aged dlPFC (31 years) react against pSer214-tau. (B) In dendritic spines, pSer214-tau aggregates over the synapse (between arrows) and the spine apparatus (pink-pseudocolored). (C) Tau fibrillation, revealed with the AT8 antibody, is sporadic in the aged dlPFC (33 years). (D and E) AT8-reactive PHFs with 80-nm helix periodicity (parallel bars in D) and abrupt endings (white arrowheads in E) as PHFs in AD. Red arrowheads point to pSer214-tau (A and B) or PHF-tau (C—E). Scale bars, 20 μm (A and C), 200 nm (B), 80 nm (D), and 40 nm (E). (F and G) Immunoblotting of tau shows more advanced phosphorylation state in the ERC than dlPFC, reflected by both increased tau at higher molecular weights (F) and increasing insolubility, S3/S1 (G). Changes in solubility are not observed across a similar age range in the dlPFC. Total tau was normalized to total protein (Supplementary Figs. 6 and 7). Abbreviations: AD, Alzheimer's disease; Ax, axon; dlPFC, dorsolateral prefrontal cortex; ERC, entorhinal cortex; NFTs, neurofibrillary tangles; PHF, paired helical filament; pSer214-tau, protein kinase A-phos-phorylated tau; Sp, spine.
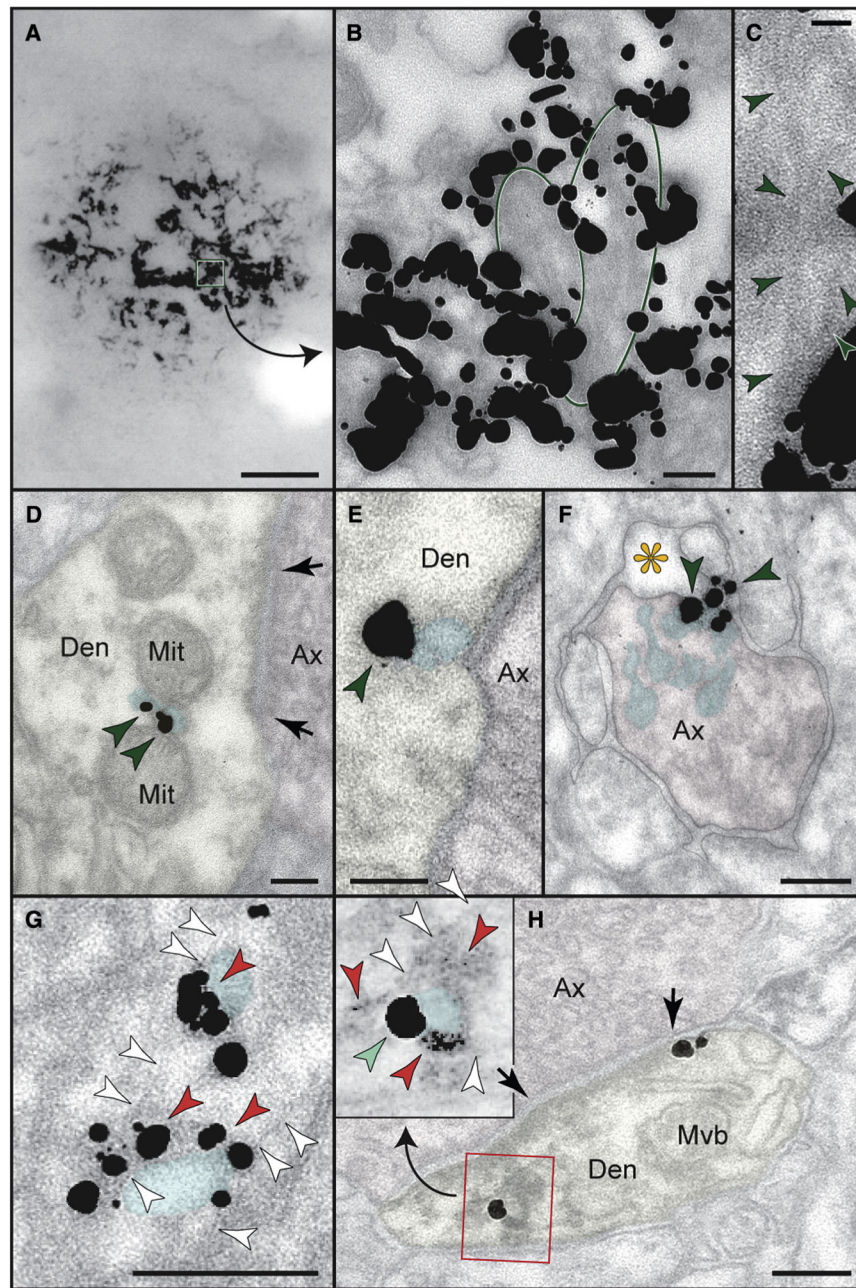
Fig. 5.
Amyloid pathology in the aged macaque ERC (33–34 years). (A) A senile plaque is labeled against Aβ. (B and C) The plaque forms extracellularly and contains cell debris and a fibrous core (green ovals); enlarged in (C) to show individual Aβ fibrils (green arrowheads). (D–F) Intracellular Aβ (green arrowheads) is captured in endosomes (cyan-pseudocolored) in axons and dendrites. Note the Aβ-loaded endosomes next to the axonal plasma membrane (traced for clarity) in (F) and the accumulation of Aβ in the widened intercellular space (yellow asterisk). (G) Fibrils (white arrowheads) labeled with AT8 against PHF-tau (red arrowheads) surround endosomes (cyan-pseudocolored). (H) An APP-transporting endosome (immunogold; light green arrowhead) is surrounded by fibrils (white arrowheads)

and PHF-tau aggregates (immunoperoxidase; red arrowheads). Synapses are between arrows. Scale bars, 20 μm (A), 200 nm (B and D–H), 30 nm (C). Abbreviations: Aβ, amyloid β; APP, amyloid precursor protein; Ax, axon; Den, dendrite; ERC, entorhinal cortex; Mit, mitochondrion; Mvb, multivesicular body; PHF, paired helical filament.
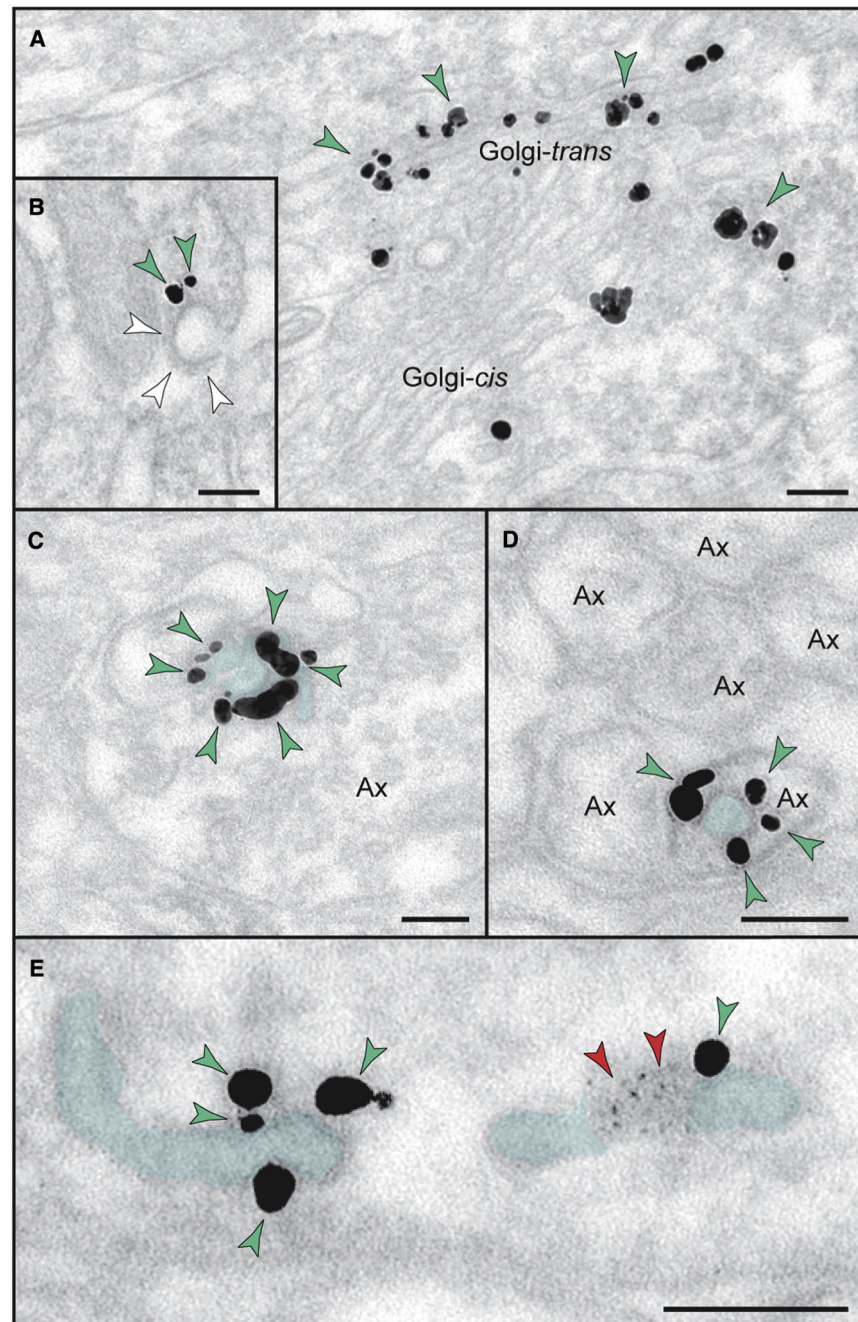
Fig. 6.
APP trafficking visualized *in situ* in the aged macaque dlPFC (33–34 years). (A) Detail of the soma of a layer III pyramidal neuron showing APP in the trans-Golgi network. (B) APP, which is internalized into endosomes via clathrin-mediated endocytosis, is captured in a clathrin-coated pit (white arrowheads point to the clathrin lattice); the labeled C-terminus protrudes intracellularly. (C and D) APP-transporting endosomes (cyan-pseudocolored) in an axon terminal (C) and a preterminal, that is, intervaricose, axon (D). (E) High-power magnification of tubular endosomes (cyan-pseudocolored) labeled against APP; the gold-tagged C-terminus is on the cytoplasmic face. The endosome on the right is curved so that

its middle portion is out of the section plane. This portion corresponds to the surface of the endosome and reacts with the AT8 antibody, which shows accumulation of PHF-tau (red arrowheads). This fortunate section plane captures the direct interaction of fibrillated tau aggregates with a single APP-transporting endosome. Scale bars, 100 nm (A–E). Abbreviations: APP, amyloid precursor protein; Ax, axon; dlPFC, dorsolateral prefrontal cortex; PHF, paired helical filament.